Equation of state of nuclear and neutron matter at third-order in perturbation theory from chiral effective field theory

J. W. Holt[1] and N. Kaiser[2]

[1]*Cyclotron Institute and Department of Physics and Astronomy, Texas A&M University, College Station, Texas 77843, USA*

[2]*Physik Department, Technische Universität München, D-85747 Garching, Germany*

(Received 15 December 2016; revised manuscript received 22 February 2017; published 29 March 2017)

We compute from chiral two- and three-nucleon interactions the energy per particle of symmetric nuclear matter and pure neutron matter at third-order in perturbation theory including self-consistent second-order single-particle energies. Particular attention is paid to the third-order particle-hole ring diagram, which is often neglected in microscopic calculations of the equation of state. We provide semianalytic expressions for the direct terms from central and tensor model-type interactions that are useful as theoretical benchmarks. We investigate uncertainties arising from the order-by-order convergence in both many-body perturbation theory and the chiral expansion. Including also variations in the resolution scale at which nuclear forces are resolved, we provide new error bands on the equation of state, the isospin-asymmetry energy, and its slope parameter. We find in particular that the inclusion of third-order diagrams reduces the theoretical uncertainty at low densities, while in general the largest error arises from omitted higher-order terms in the chiral expansion of the nuclear forces.

DOI: 10.1103/PhysRevC.95.034326

I. INTRODUCTION

The nuclear isospin-asymmetry energy $S(\rho)$, defined as the difference between the energy per particle of homogeneous neutron matter and symmetric nuclear matter at a given density ρ, offers important links between the properties of terrestrial nuclei and extreme astrophysical systems such as core-collapse supernovae, neutron stars, and neutron star mergers [1–3]. Clarifying the experimental and theoretical uncertainties on the isospin-asymmetry energy is therefore an important objective in contemporary low-energy nuclear physics. Intermediate-energy heavy-ion collision experiments [4–7] can access the equation of state of nuclear matter at suprasaturation densities, and modern theoretical methods such as chiral effective field theory (EFT) [8–10] and the renormalization group [11,12] allow for nuclear matter calculations with reliable uncertainty estimates up to roughly $\rho \simeq 2\rho_0$, where $\rho_0 \simeq 0.16\,\mathrm{fm}^{-3}$ is the saturation density. These estimates are achieved through systematic studies [13,14] of the order-by-order convergence in the chiral power counting together with variations in the resolution scale [15] and low-energy constants [16] in the chiral two-body ($2N$) and three-body ($3N$) potentials. In addition, the comparison of different perturbative [17–20] and nonperturbative methods [21–27] for solving the nuclear many-body problem starting from identical Hamiltonians can give insight into additional sources of error. In all cases, both theoretical and experimental uncertainty bands grow rapidly with the density beyond $\rho = \rho_0$. In the vicinity of nuclear matter saturation density, microscopic calculations [28,29] of the isospin-asymmetry energy $S(\rho)$ and its slope parameter L tend to lie just outside of the experimental band [30,31]. More detailed investigations of theoretical uncertainties may therefore shed light on this discrepancy.

In the present work, we explore the role of third-order perturbative contributions to the nuclear and neutron matter equations of state as well as the effects of self-consistent second-order single-particle energies. Numerous works [18,19,32,33] have studied the importance of particle-particle and hole-hole ladder diagrams at third-order, but the third-order particle-hole diagram is often neglected due to its more complicated momentum and spin recouplings when expressed in terms of partial waves, which significantly increase the computational cost. In Ref. [20] it was found that the third-order particle-hole diagram gives a contribution on the order of $|E^{(3)}_{\mathrm{ph}}(\rho_0)| \sim (1\text{-}2)\,\mathrm{MeV}$ in symmetric nuclear matter when computed from coarse-resolution chiral NN potentials with momentum-space cutoffs $\Lambda \lesssim 500\,\mathrm{MeV}$. Third-order contributions are expected to be less important in neutron matter, which generally exhibits faster convergence [34,35] in many-body perturbation theory, but to date no works have computed all third-order diagrams in neutron matter with three-body forces included. Moreover, single-particle propagators are often treated at the (first-order) Hartree-Fock level, which introduces a strong momentum dependence in the mean-field potential that reduces the second- and third-order diagrammatic contributions to the energy per particle by up to 30% and 50%, respectively, at nuclear matter saturation density. However, it is well known [16,36,37] that second-order perturbative contributions to the nucleon self-energy in nuclear matter from two-body forces [38] reduce the momentum dependence of the single-particle potential in the vicinity of the Fermi surface. A conservative estimate of this uncertainty can therefore be obtained by employing both a free-particle spectrum and a Hartree-Fock spectrum [33]. An additional aim of the present work is to reduce this significant source of uncertainty.

We employ as a starting point realistic NN potentials at different orders $\{(q/\Lambda_\chi)^2,(q/\Lambda_\chi)^3,(q/\Lambda_\chi)^4\}$ in the chiral expansion, corresponding to next-to-leading order (NLO), next-to-next-to-leading order (N2LO), and next-to-next-to-next-to-leading order (N3LO). The short-range contact terms

are fitted to elastic nucleon-nucleon scattering phase shifts and deuteron properties, while the intermediate- and long-range interactions are determined uniquely by one- and multi-pion exchange processes constrained by chiral symmetry. We vary the momentum-space cutoff Λ, which sets the scale at which nuclear forces are resolved, over the range $\Lambda \simeq$ (400-500) MeV [39–41], which is suitable for many-body perturbation theory calculations of the energy density. We include as well the chiral three-nucleon force at order $(q/\Lambda_\chi)^3$, which is fitted to the binding energy and β-decay lifetime of ^3H [13]. Extension to a consistent treatment at order $(q/\Lambda_\chi)^4$ requires the refitting of the c_D and c_E low-energy constants, which is currently a work in progress. In the following we refer to this partly incomplete treatment at order $(q/\Lambda_\chi)^4$ as N3LO*. The coarse-resolution chiral potentials employed in the present work have also been used to study the response functions of neutron matter [42] as well as numerous thermodynamic properties of symmetric nuclear matter and neutron matter [43] (for recent reviews see Refs. [44,45]).

The present paper is organized as follows. In Sec. II we outline the calculation of the ground-state energy density of symmetric nuclear matter and pure neutron matter at third-order in perturbation theory, including self-consistent single-particle spectra. As a benchmark for the complicated partial-wave decomposition of the third-order particle-hole ring diagram for realistic NN potentials, we present semi-analytic results for the direct terms from central and tensor model-type interactions. In Sec. III we present a comprehensive study of the theoretical uncertainties for the equation of state of symmetric nuclear matter and pure neutron matter. We extract the isospin-asymmetry energy S_0 and its slope parameter L at saturation density, including also the results from nuclear forces at NLO and N2LO in the chiral power counting. Furthermore, the third-order particle-hole diagrams from an S-wave contact interaction (with two parameters a_s and a_t) allow us to examine the commonly used quadratic approximation in the isospin-asymmetry. We end with a summary and conclusions.

II. ENERGY PER PARTICLE AT THIRD ORDER IN PERTURBATION THEORY

The first-, second-, and third-order perturbative contributions to the energy density of nuclear (or neutron) matter are shown diagrammatically in Fig. 1. The wavy line represents the (antisymmetrized) density-dependent NN interaction as given by the sum of the free-space NN potential and the in-medium NN interaction derived from the N2LO chiral three-nucleon force. The latter is obtained by closing two external legs and summing over the filled Fermi sea of (free) nucleons [16,46]. The method is equivalent to constructing a normal-ordered Hamiltonian with respect to the noninteracting ground state and neglecting the residual three-body contribution [47]. This approximation has been improved in other works by including three-body forces at N3LO [48] and by keeping the residual three-body force after normal ordering [33,49]. The first-, second-, and third-order contributions to the energy density ρE (with ρ being the density and E the energy per particle)

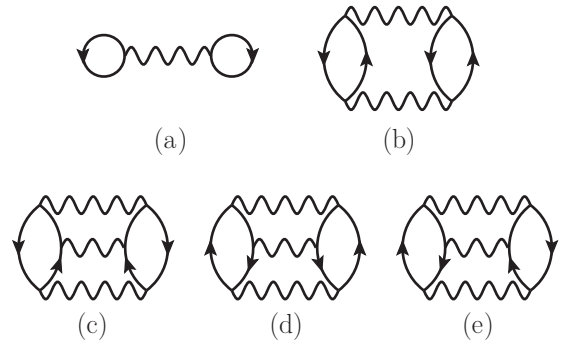

FIG. 1. First-, second-, and third-order diagrammatic contributions to the ground-state energy density of isospin-symmetric nuclear matter and pure neutron matter from the (effective) chiral two-nucleon potential described in the text. The wavy line includes the (antisymmetrized) density-dependent NN interaction derived from the chiral three-body force at N2LO.

are given by

$$\rho E^{(1)} = \frac{1}{2}\sum_{12} n_1 n_2 \langle 12 | \big(\overline{V}_{NN} + \overline{V}^{\rm med}_{NN}/3\big) | 12\rangle, \tag{1}$$

$$\rho E^{(2)} = -\frac{1}{4}\sum_{1234} |\langle 12|\overline{V}_{\rm eff}|34\rangle|^2 \frac{n_1 n_2 \bar{n}_3 \bar{n}_4}{e_3 + e_4 - e_1 - e_2}, \tag{2}$$

$$\rho E^{(3)}_{\rm pp} = \frac{1}{8}\sum_{123\,456} \langle 12|\overline{V}_{\rm eff}|34\rangle\langle 34|\overline{V}_{\rm eff}|56\rangle\langle 56|\overline{V}_{\rm eff}|12\rangle \times \frac{n_1 n_2 \bar{n}_3 \bar{n}_4 \bar{n}_5 \bar{n}_6}{(e_3 + e_4 - e_1 - e_2)(e_5 + e_6 - e_1 - e_2)}, \tag{3}$$

$$\rho E^{(3)}_{\rm hh} = \frac{1}{8}\sum_{123\,456} \langle 12|\overline{V}_{\rm eff}|34\rangle\langle 34|\overline{V}_{\rm eff}|56\rangle\langle 56|\overline{V}_{\rm eff}|12\rangle \times \frac{\bar{n}_1 \bar{n}_2 n_3 n_4 n_5 n_6}{(e_1 + e_2 - e_3 - e_4)(e_1 + e_2 - e_5 - e_6)}, \tag{4}$$

$$\rho E^{(3)}_{\rm ph} = -\sum_{123\,456} \langle 12|\overline{V}_{\rm eff}|34\rangle\langle 54|\overline{V}_{\rm eff}|16\rangle\langle 36|\overline{V}_{\rm eff}|52\rangle \times \frac{n_1 n_2 \bar{n}_3 \bar{n}_4 n_5 \bar{n}_6}{(e_3 + e_4 - e_1 - e_2)(e_3 + e_6 - e_2 - e_5)}, \tag{5}$$

where $n_j = \theta(k_f - |\vec{p}_j|)$ is the (steplike) distribution function, $\bar{n}_j = 1 - n_j$, and $\overline{V} = V - \mathcal{P}_{12}V$ is the (Fierz) antisymmetrized NN potential, with $\mathcal{P}_{12}$ being the exchange-operator in spin-, isospin-, and momentum-space. The effective NN potential is given by the sum $V_{\rm eff} = V_{NN} + V^{\rm med}_{NN}$. Note that the third-order particle-particle and hole-hole Goldstone diagrams have a symmetry factor of $\frac{1}{8} = \frac{1}{2^3}$ arising from three pairs of equivalent lines, while the third-order particle-hole diagram has no equivalent pairs of lines and consequently an overall symmetry factor of 1.

The third-order particle-particle and hole-hole contributions can be straightforwardly decomposed in terms of partial-wave matrix elements of $\overline{V}$ and written as integrals over the relative momenta of the interacting nucleons. The third-order particle-hole contribution, on the other hand, is more conveniently calculated by integrating over the individual

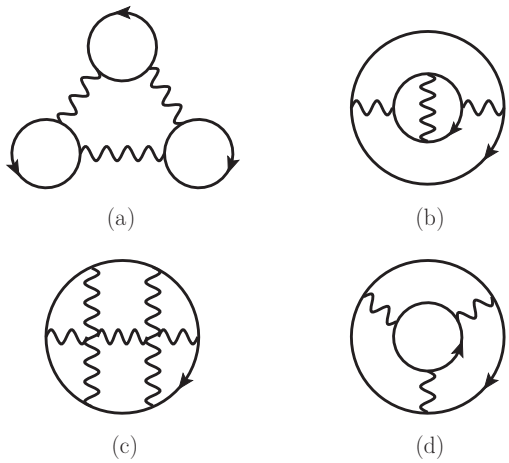

FIG. 2. Four ring diagrams representing the third-order particle-hole contribution, organized according to the number of direct and exchange interactions. Diagrams (a), (b), (c), and (d) have 0, 1, 2, and 3 exchange interactions, respectively.

particle-momenta, which however leads to more complicated expressions when written in terms of partial-wave matrix elements. We therefore provide semianalytical expressions for several of the third-order particle-hole ring diagrams from model-type interactions, which are useful to benchmark the results of extensive numerical calculations. We begin by decomposing the third-order particle-hole ring contribution into four parts, shown in Fig. 2, according to the number of direct (dir) and exchange (exch) interactions. We denote diagram (a) in Fig. 2 as the dir^3 term, diagram (b) as the $\mathrm{dir}^2 \cdot \mathrm{exch}$ term, diagram (c) as the $\mathrm{dir} \cdot \mathrm{exch}^2$ term, and diagram (d) as the exch^3 term. We have computed all contributions (a)–(d) for various model-type interactions and one-pion exchange, but the parts involving multiple exchange terms lead to very lengthy expressions, and for brevity we present the semianalytic results here only for diagrams (a) and (b) in Fig. 2.

We consider first a scalar isoscalar boson-exchange interaction of the form

$$V_{\mathrm{dir}}(q) = -\frac{g^2}{m^2+q^2}, \tag{6}$$

with q being the momentum transfer. The contribution to the energy per particle $E(\rho)$ of symmetric nuclear matter from diagram $(a) = \mathrm{dir}^3/6$ is given by

$$E(\rho)^{(\mathrm{a})} = -\frac{g^6M^2}{32\pi^7 k_f}\int_0^\infty ds\int_0^\infty d\kappa\left[\frac{Q_0(s,\kappa)}{s^2+\beta}\right]^3, \tag{7}$$

where M is the nucleon mass, $\beta = m^2/4k_f^2$, and the Fermi momentum is related to the density by $\rho = 2k_f^3/3\pi^2$. The (Euclidean) polarization function $Q_0(s,\kappa)$, arising from an individual nucleon ring in diagram (a) of Fig. 2, has the following analytical form:

$$\begin{aligned} Q_0(s,\kappa) = {} & s - s\kappa\arctan\frac{1+s}{\kappa} - s\kappa\arctan\frac{1-s}{\kappa} \\ & + \frac{1}{4}(1-s^2+\kappa^2)\ln\frac{(1+s)^2+\kappa^2}{(1-s)^2+\kappa^2}. \end{aligned} \tag{8}$$

The contribution to the energy per particle of symmetric nuclear matter from diagram $(b) = -\mathrm{dir}^2 \cdot \mathrm{exch}/2$ can be represented by a sixfold integral:

$$\begin{aligned} E(\rho)^{(\mathrm{b})} = {} & \frac{6g^6M^2}{(2\pi)^7 k_f}\int_0^\infty ds\int_0^\infty d\kappa\int_0^1 dl_1\int_0^1 dl_2\int_{-l_1}^{l_1} dx \\ & \times\int_{-l_2}^{l_2} dy\,\frac{l_1 l_2\, Q_0(s,\kappa)\,(s^2+\beta)^{-2}}{[(s+x)^2+\kappa^2][(s+y)^2+\kappa^2]} \\ & \times\Big\{[(s+x)(s+y)-\kappa^2] \\ & \times W_a^{-1/2} + [(s+x)(s+y)+\kappa^2]W_b^{-1/2}\Big\}, \end{aligned} \tag{9}$$

with the auxiliary functions $W_a = [4\beta + l_1^2 + l_2^2 - 2xy]^2 - 4(l_1^2-x^2)(l_2^2-y^2)$ and $W_b = [4\beta + l_1^2 + l_2^2 + 4s(s+x+y) + 2xy]^2 - 4(l_1^2-x^2)(l_2^2-y^2)$.

For a modified pseudoscalar isovector boson-exchange interaction of the form

$$V_{\mathrm{dir}} = -g^2\vec{\tau}_1\cdot\vec{\tau}_2\,\frac{\vec{\sigma}_1\cdot\vec{q}\,\vec{\sigma}_2\cdot\vec{q}}{(m^2+q^2)^2}, \tag{10}$$

the contribution to the energy per particle of symmetric nuclear matter from diagram $(a) = \mathrm{dir}^3/6$ reads

$$E(\rho)^{(\mathrm{a})} = -\frac{3g^6M^2}{32\pi^7 k_f}\int_0^\infty ds\int_0^\infty d\kappa\left[\frac{s^2 Q_0(s,\kappa)}{(s^2+\beta)^2}\right]^3. \tag{11}$$

The contribution to the energy per particle of symmetric nuclear matter from diagram $(b) = -\mathrm{dir}^2 \cdot \mathrm{exch}/2$ is on the other hand given by

$$\begin{aligned} E(\rho)^{(\mathrm{b})} = {} & \frac{18g^6M^2}{(2\pi)^7 k_f}\int_0^\infty ds\int_0^\infty d\kappa\int_0^1 dl_1\int_0^1 dl_2\int_{-l_1}^{l_1} dx\int_{-l_2}^{l_2} dy\,\frac{l_1 l_2 s^4\, Q_0(s,\kappa)\,(s^2+\beta)^{-4}}{[(s+x)^2+\kappa^2][(s+y)^2+\kappa^2]}\big([(s+x)(s+y)-\kappa^2] \\ & \times\big[4\beta\big(l_1^2+l_2^2-2x^2-2y^2+2xy\big)+\big(l_1^2-l_2^2-2x^2+2xy\big)\big(l_1^2-l_2^2+2y^2-2xy\big)\big]W_a^{-3/2} + [(s+x)(s+y)+\kappa^2] \\ & \times\big\{4\beta\big[l_1^2+l_2^2-4s(s+x+y)-2x^2-2y^2-2xy\big]+\big[l_1^2-l_2^2-4s(s+x+y)-2x(x+y)\big] \\ & \times\big[l_1^2-l_2^2+4s(s+x+y)+2y(x+y)\big]\big\}W_b^{-3/2}\big). \end{aligned} \tag{12}$$

In Fig. 3 we compare the sum of all four contributions, $(a)+(b)+(c)+(d)$, to the third-order particle-hole diagram in symmetric nuclear matter from the two test interactions in Eqs. (6) and (10) employing both a partial-wave decomposition

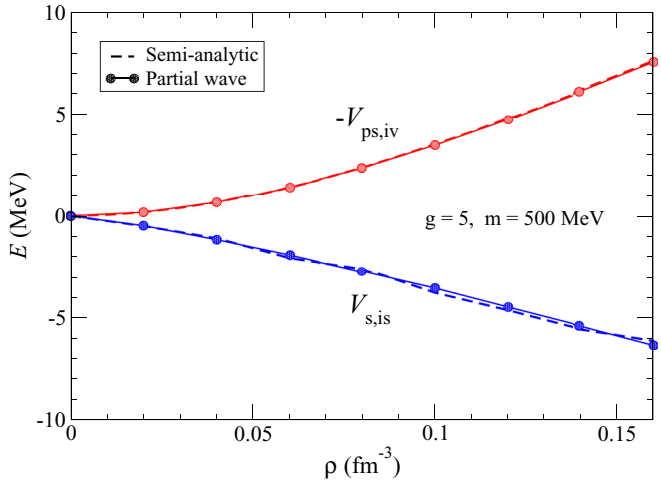

FIG. 3. The density dependence of the third-order particle-hole contribution to the ground-state energy per particle, E, of symmetric nuclear matter from the scalar-isoscalar test interaction in Eq. (6) and the modified pseudoscalar-isovector test interaction in Eq. (10). The contribution from the latter is multiplied by -1 for better clarity in the figure. The results of numerical calculations based on a partial-wave decomposition are shown together with semi-analytic results involving only multidimensional integrals.

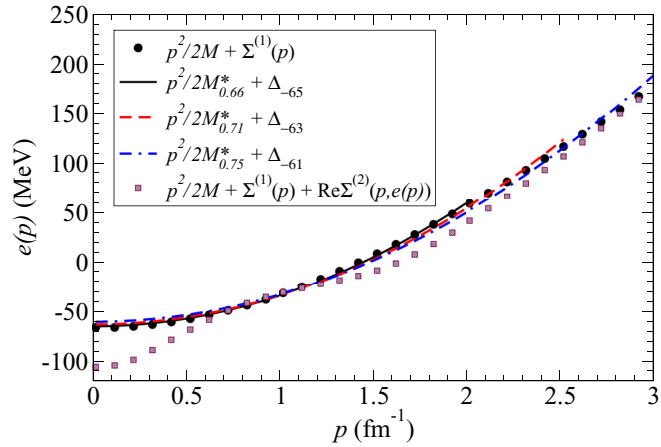

FIG. 4. Nucleon single-particle energy in symmetric nuclear matter at saturation density including the first-order $\Sigma^{(1)}$ and second-order $\Sigma^{(2)}$ perturbative contributions to the self-energy. The effective mass and energy shift parametrization is shown for three different choices of the fitting region in momentum space, and the values of the effective mass (M^*/M) and the energy shift Δ (in units of MeV) are shown as subscripts.

(used in Sec. III below for realistic chiral two- and three-nucleon forces) and a semianalytic evaluation. The boson mass is taken to be $m = 500\,\mathrm{MeV}$ for both interactions and the coupling constant is chosen to be $g = 5$. For the modified pseudoscalar-isovector force model, labeled $V_{\mathrm{ps,iv}}$ in Fig. 3, we have changed the overall sign of the interaction to more easily differentiate the two terms in the figure. We see from Fig. 3 that the two sets of calculations agree almost perfectly. In the case of the scalar-isoscalar test interaction, large cancellations among the four terms computed with the semianalytic method result in numerical noise on the order of (4–8)% relative to the results from the partial-wave decomposition. In comparison, the two methods agree to within 1% across all densities for the energy per particle of symmetric nuclear matter from the modified isovector-pseudoscalar test interaction. A further case to check our numerical calculations is given by the third-order ring contributions from an S-wave contact interaction of the form $V_{\mathrm{ct}} = -\frac{\pi}{M}[a_s + 3a_t + (a_t - a_s)\vec{\sigma}_1 \cdot \vec{\sigma}_2]$. Using the polarization function $Q_0(s,\kappa)$ in Eq. (8) and integrating over its cube, one finds for symmetric nuclear matter

$$E(\rho) = 1.04814\,\frac{k_f^5}{\pi^4 M}(a_s + a_t)\big(5a_s^2 - 14a_s a_t + 5a_t^2\big) \quad (13)$$

and for pure neutron matter

$$E_n(\rho_n) = 2.79505\,\frac{k_n^5}{\pi^4 M}a_s^3, \quad (14)$$

with k_n being the neutron Fermi momentum related to the neutron density by $\rho_n = k_n^3/3\pi^2$. For various choices of the scattering lengths a_s and a_t, we reproduce these results with an accuracy of 1% and better.

Until now we have assumed a free-particle spectrum for the single-particle energies occurring in the denominators of the second- and third-order perturbative contributions to the equation of state. For calculations involving high-precision chiral two- and three-body forces, it is convenient to employ Hartree-Fock single-particle energies, which are well approximated by the effective mass M^* plus energy shift Δ parametrization:

$$e(p) = \frac{p^2}{2M^*} + \Delta, \quad (15)$$

where Δ is independent of the momentum p. At the mean-field level, the single-particle potential has a strong momentum dependence that gives rise to nucleon effective masses in the vicinity of $M^*/M \simeq 0.7$ at nuclear matter saturation density. This leads to a reduction of the second-order energy contribution in Eq. (2) by roughly 30%. All third-order contributions are likewise scaled by $(M^*/M)^2 \simeq 0.5$ at nuclear saturation density. A second-order perturbative treatment of the nucleon self-energy in symmetric nuclear matter, however, gives rise to an effective mass that is itself strongly momentum dependent, and the parametrization in Eq. (15) is no longer valid. In particular, close to the Fermi momentum the effective mass peaks at a value close to the free-space mass [36]. The associated uncertainty in the symmetric nuclear matter equation of state at saturation density is on the order of 5 MeV [20] while for neutron matter the uncertainty is 2–3 MeV [19].

In Fig. 4 we show the nucleon single-particle energy in nuclear matter at saturation density calculated at the Hartree-Fock level, $e(p) = p^2/2M + \Sigma^{(1)}(p)$, together with three different effective mass plus energy shift parametrizations fitted over the ranges in momentum: $p < 2.0\,\mathrm{fm}^{-1}$, $p < 2.5\,\mathrm{fm}^{-1}$, and $p < 3.0\,\mathrm{fm}^{-1}$. The subscripts on the M^* and Δ terms refer to the values of (M^*/M) and Δ (in units of MeV). The momentum dependence of the single-particle energy at the Hartree-Fock level remains nearly quadratic, but we observe

that the values of M^*/M and Δ depend on the choice of the fitting region.

In Sec. III below, we compute the single-particle energies in Eqs. (2)–(5) self-consistently at second-order:

$$e(p) = \frac{p^2}{2M} + \Sigma^{(1)}(p) + \mathrm{Re}\,\Sigma^{(2)}(p, e(p)). \qquad (16)$$

The Hartree-Fock contribution, $\Sigma^{(1)}(p)$, to the nucleon self-energy in nuclear matter depends only on the momentum and is manifestly real. The second-order contribution, $\Sigma^{(2)}(p, e(p))$, is in general complex and energy dependent. In practice Eq. (16) is solved iteratively until a converged solution is reached. The inclusion of a density-dependent two-body force derived from the leading chiral three-body force requires an additional symmetry factor of 1/2 in the Hartree-Fock contribution $\Sigma^{(1)}(p)$. For additional computational details we refer the reader to Refs. [50,51]. We show in Fig. 4 the nucleon single-particle energy in symmetric nuclear matter including also the second-order contribution $\Sigma^{(2)}(p, e(p))$ to the self-energy. In contrast to the Hartree-Fock approximation, the momentum dependence of the single-particle energy is no longer approximately quadratic.

The nucleon self-energy in infinite nuclear matter is related to the volume components of the nucleon-nucleus optical potential probed in elastic scattering experiments. If Refs. [50,51] we employed low-momentum chiral two- and three-body forces at second-order in perturbation theory and found very good agreement with the isoscalar and isovector real components of the optical potential compared to phenomenology [52–54] for energies $E \lesssim 200$ MeV.

III. RESULTS

In this section we calculate the energy per particle of symmetric nuclear matter and pure neutron matter at third-order in perturbation theory with self-consistent single-particle energies at second-order. Our aim is to provide improved theoretical error estimates on the equations of state $E(\rho)$ and $E_n(\rho_n)$, the density-dependent symmetry energy $S(\rho)$, and the slope parameter L of the symmetry energy. We account for theoretical uncertainties arising from the convergence in perturbation theory, the choice of resolution scale, and the omission of higher-order terms in the chiral expansion.

We begin with the equation of state of symmetric nuclear matter at first-order in perturbation theory, shown in Fig. 5 as a function of density for three different chiral potentials with momentum-space cutoffs of $\Lambda = (414, 450, 500)$ MeV. Each of the N3LO two-nucleon forces are supplemented with a density-dependent NN interaction constructed from the N2LO three-body force, whose low-energy constants c_D and c_E are fitted to the binding energy and lifetime of the triton. In Table I we also show the specific values of the first-order contribution (in units of MeV) at nuclear matter saturation density ρ_0. For comparison the noninteracting Fermi gas contribution [i.e., the kinetic energy $E_{\rm kin}(\rho) = 3k_f^2/10M$] at this density is $E_{\rm kin} = 22.1$ MeV. At the mean-field level there is a large uncertainty associated with the choice of resolution scale, a feature observed already in Ref. [15]. However,

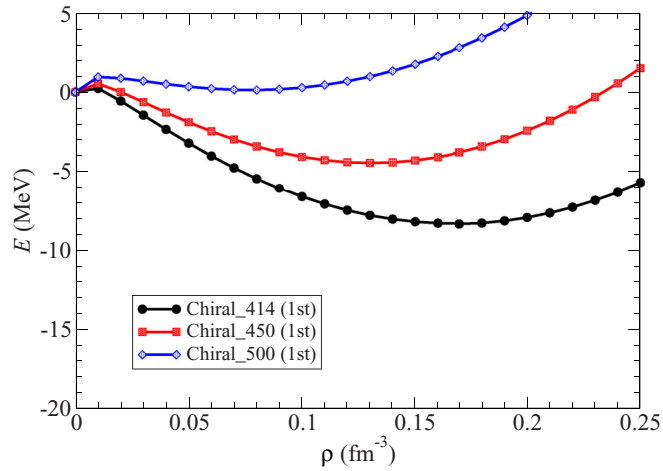

FIG. 5. First-order diagrammatic contribution to the energy per particle of symmetric nuclear matter from N3LO* chiral two- and three-nucleon forces defined at different resolution scales: $\Lambda = (414, 450, 500)$ MeV.

the error band at this order in the perturbative expansion does not pass through the empirical saturation point at $\rho_0 = 0.16\,\mathrm{fm}^{-3}$ and $E(\rho_0) = -16$ MeV, and therefore varying the resolution scale over the range typically chosen in constructing chiral potentials does not encompass the full theoretical uncertainty.

The results for the equation of state of symmetric nuclear matter including second-order perturbative contributions are shown in Fig. 6. We consider both a Hartree-Fock spectrum (labeled "2nd HF") for the intermediate-state energies and a self-consistent second-order approximation (labeled "2nd SC"). As expected, the latter leads to additional attraction resulting from a reduced momentum-dependence of the single-particle potential. The differences between the second-order contributions with a HF and a SC spectrum reach up to (2–3) MeV for densities below $\rho = 0.25\,\mathrm{fm}^{-3}$, a feature that is largely independent of the choice of resolution scale. In Table I we show the specific values at nuclear matter saturation density and include also the results, labeled $E^{(2)}$, employing a free-particle spectrum. By comparing the magnitude of

TABLE I. The contribution to the energy per particle $E(\rho_0)$ of symmetric nuclear matter from the first-, second-, and third-order perturbation theory diagrams employing chiral two- and three-nucleon forces. For the second-order contribution we list the values using a free single-particle spectrum, $E^{(2)}$, a Hartree-Fock spectrum, $E^{(2\mathrm{HF})}$, and self-consistent single-particle energies at second-order, $E^{(2\mathrm{SC})}$. All values are in units of MeV and the noninteracting contribution (not included) is $E_{\rm kin} = 22.1$ MeV.

		$E^{(2)}$			$E^{(3)}$		
Λ	$E^{(1)}$	$E^{(2)}$	$E^{(2\mathrm{HF})}$	$E^{(2\mathrm{SC})}$	$E^{(3\mathrm{SC})}_{\rm pp}$	$E^{(3\mathrm{SC})}_{\rm hh}$	$E^{(3\mathrm{SC})}_{\rm ph}$
414	−30.1	−11.0	−7.9	−9.7	0.8	−0.3	−0.3
450	−25.9	−15.9	−11.5	−13.2	1.0	−0.2	−1.5
500	−19.5	−18.7	−13.3	−15.7	2.2	−0.1	−2.1

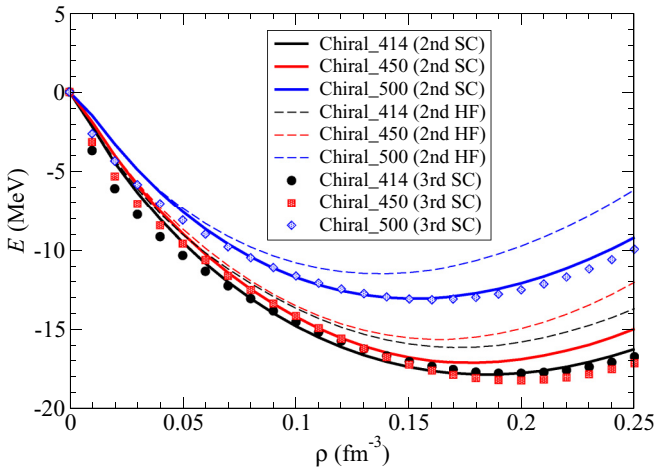

FIG. 6. The equation of state of symmetric nuclear matter at second- and third-order in many-body perturbation theory from N3LO* chiral two- and three-body forces. Both a Hartree-Fock (HF) spectrum and a self-consistent (SC) second-order single-particle spectrum were employed for the three chiral potentials with different momentum-space regulator scales.

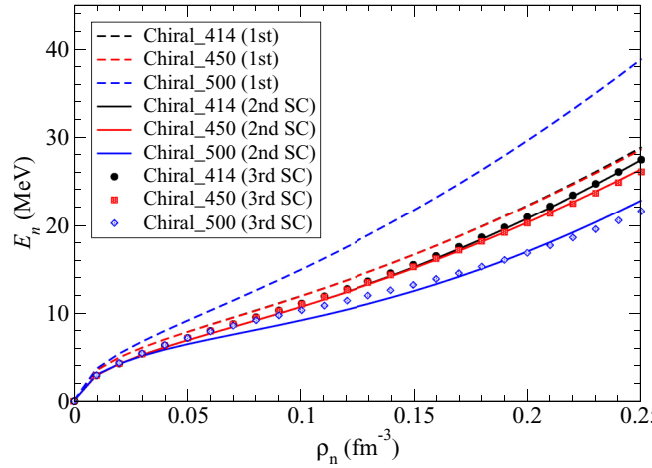

FIG. 7. Neutron matter equation of state at first-, second-, and third-order in many-body perturbation theory from N3LO* chiral two- and three-nucleon forces. For both the second- and third-order contributions, the nucleon self-energies are computed self-consistently (SC) at second-order. Results are shown for chiral potentials constructed with a range of momentum-space cutoffs: $\Lambda = (414,450,500)$ MeV.

the second-order contributions $E^{(2SC)}$ to the leading-order Hartree-Fock contributions $E^{(1)}$ at nuclear matter saturation density, we observe an improved convergence pattern as the momentum-space cutoff Λ is lowered. At second-order in perturbation theory, the error estimate obtained through varying the cutoff scale now encompasses the empirical saturation point.

The third-order contributions to the energy per particle of symmetric nuclear matter, with single-particle energies computed self-consistently at second-order, are shown in Fig. 6 and labeled "3rd SC." We observe that taken together the three contributions $E^{(3)}_{\rm pp}$, $E^{(3)}_{\rm hh}$, and $E^{(3)}_{\rm ph}$ give rise to additional attraction at both low and high densities. In particular, for densities less than $\rho \simeq 0.08\,{\rm fm}^{-3}$, where a spinodal instability is expected [55], the third-order terms cannot be neglected. At and above saturation density, the perturbation theory expansion appears to be better converged, though generically both repulsive particle-particle and attractive particle-hole contributions are individually on the order of (1–3) MeV. In Table I we show the values of the three third-order contributions at nuclear matter saturation density including self-consistent second-order single-particle energies, for each of the three chiral potentials considered in this section. Given the systematic cancellations that occur between the third-order particle-particle and particle-hole diagrams (independent of resolution scale Λ), we suggest that these terms should be included together or not at all. From Fig. 6 we see that the largest source of theoretical uncertainty comes from the choice of resolution scale, as was found previously in Ref. [13]. The empirical saturation point is nearly at the central value of the error band, but there remains a $\Delta E \simeq 6\,{\rm MeV}$ uncertainty in the energy per particle at $\rho = \rho_0$.

We next consider the equation of state of pure neutron matter from chiral two- and three-nucleon forces at order N3LO*. In Fig. 7 we show the results at first-, second-, and third-order in perturbation theory from chiral potentials with momentum-space cutoffs $\Lambda = (414,450,500)$ MeV. At leading-order in perturbation theory there is again a large dependence on the choice of resolution scale, but at both second- and third-order the variations are about $\Delta E_n \simeq 2\,{\rm MeV}$ at $\rho_n = 0.16\,{\rm fm}^{-3}$ and $\Delta E_n \simeq 3\,{\rm MeV}$ at $\rho_n = 0.25\,{\rm fm}^{-3}$. The inclusion of the third-order diagrams has relatively little effect for the chiral potentials with $\Lambda = 414$ MeV and 450 MeV, which we see give nearly identical equations of state at each order in perturbation theory across all densities considered. In contrast, the equation of state from the $\Lambda = 500\,{\rm MeV}$ potential receives important contributions at low densities that significantly reduce the scale dependence. In fact, for densities up to $\rho_n \simeq 0.10\,{\rm fm}^{-3}$, all N3LO* chiral potentials give a nearly unique neutron matter equation of state. At higher densities the third-order contributions do not reduce the scale dependence in any meaningful way.

Theoretical uncertainties on the neutron matter equation of state estimated from the convergence pattern of many-body perturbation theory and variations in the resolution scale are relatively small. The error estimates on the density-dependent isospin-asymmetry energy, defined as the difference $S(\rho) = E_n(\rho) - E(\rho)$, are correspondingly tight, similar to what has already been reported in previous studies with microscopic two- and three-body forces [28,29], which predict values of the isospin-asymmetry energy and the slope parameter that lie just outside of the experimental uncertainty band [30,31]. To better understand this discrepancy we consider now the errors due to neglected higher-order contributions in the chiral expansion. In particular, three- and four-body forces at N3LO are neglected in the present treatment as well as N4LO two- and many-body forces. The two-body forces at N4LO have been shown to improve significantly in

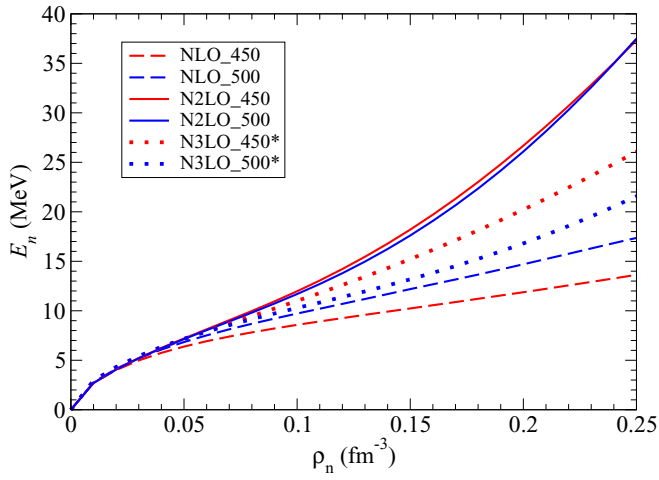

FIG. 8. Order-by-order convergence pattern of the neutron matter equation of state from NLO, N2LO, and N3LO* chiral two- and three-body potentials at third-order in many-body perturbation theory with self-consistent second-order single-particle energies. Two momentum-space cutoffs were chosen: $\Lambda = 450$ MeV and 500 MeV.

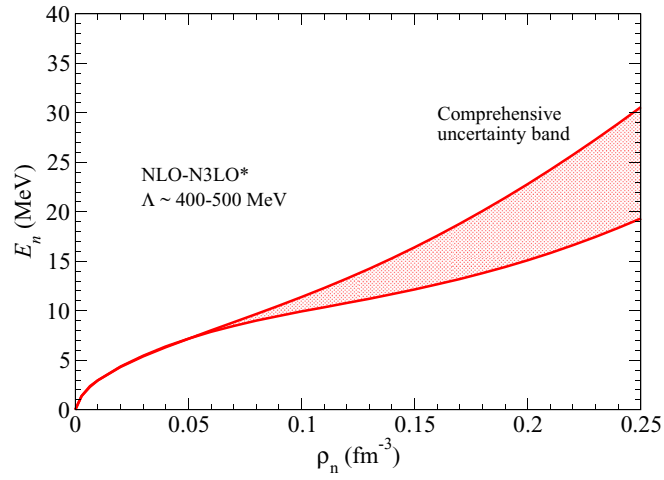

FIG. 9. Theoretical uncertainty estimate for the neutron matter equation of state from chiral effective field theory, including errors arising from the convergence in many-body perturbation theory, missing terms in the chiral expansion, and choice of resolution scale.

particular the NN-scattering phase shifts in F and G partial waves [56].

We show in Fig. 8 the equation of state calculated at third-order in perturbation theory from the NLO, N2LO, and N3LO* chiral potentials with two choices of the momentum-space regulating scale: $\Lambda = 450$ MeV and 500 MeV. In all cases the low-energy constants in the chiral two-body force are refitted [41] as a function of Λ to NN-scattering phase shifts and deuteron properties. As originally observed in Ref. [13] there is a large change from NLO to N2LO and also from N2LO to N3LO*, indicating that neglected contributions may be a very significant source of theoretical uncertainty. Comparing the ratio of differences $R_4^\Lambda = (E_n^{(4)} - E_n^{(3)})/(E_n^{(3)} - E_n^{(2)})$ for the two sets of chiral potentials, where $E_n^{(i)}$ is the neutron matter energy per particle at order $(q/\Lambda_\chi)^i$, we find that $R_4^{450} \simeq 0.4$ and $R_4^{500} \simeq 0.8$ for all but the lowest densities.

In Fig. 9 we show a comprehensive theoretical uncertainty estimate for the neutron matter equation of state that accounts for errors due to truncations in many-body perturbation theory, missing terms in the chiral effective field theory expansion, and the choice of resolution scale. The largest source of error in the present analysis is estimated to arise from missing higher-order contributions in chiral EFT. We have used the values of R_4^{450} and R_4^{500} to calculate associated error bands on the N3LO* equations of state according to $E^\Lambda_{\mathrm{N3LO}*} \pm R_4^\Lambda (E_n^{(4)} - E_n^{(3)})$. In the case of the N3LO* chiral potential with $\Lambda = 500$ MeV, the lower band on the equation of state computed according to the above prescription would be well below even NLO results which include no repulsive three-body forces. We therefore limit the lower band of the uncertainty estimate by the scale dependence error, namely, $E^{500}_{\mathrm{N3LO}*} - (E^{450}_{\mathrm{N3LO}*} - E^{500}_{\mathrm{N3LO}*})/2$. In comparison to a recent calculation [33] of the neutron matter equation of state and associated uncertainty estimate, our results exhibit a smaller theoretical error at low densities but comparable uncertainties beyond $\rho = \rho_0$. The reduction in the low-density error is directly attributed in the present calculation to the inclusion of third-order perturbative contributions.

Theoretical predictions for the isospin-asymmetry energy and its density dependence can be extracted directly from our equations of state of symmetric nuclear matter and pure neutron matter. However, due to the large uncertainties in the symmetric matter equation of state, it is more reliable to instead expand about the known empirical saturation point at $\rho_0 = 0.16\,\mathrm{fm}^{-3}$ and $E(\rho_0) = -16$ MeV. We consider the three neutron matter equations of state calculated at third-order in perturbation theory employing N3LO* chiral two- and three-body potentials. We include as well the minimum and maximum on the uncertainty band shown in Fig. 9. This gives a total of five neutron matter equations of state from which we extract the isospin-asymmetry energy at saturation density, $S_0 = S(\rho_0)$, and the associated slope parameter,

$$L = 3\rho_0 \left.\frac{\partial S(\rho)}{\partial \rho}\right|_{\rho_0}. \tag{17}$$

In Fig. 10 we show the correlation between L and S_0 computed from NLO, N2LO, and N3LO* chiral two- and three-body forces at third-order in many-body perturbation theory. The error bars on individual points are obtained by varying the saturation density between $\rho_0 = 0.155\,\mathrm{fm}^{-3}$ and $0.165\,\mathrm{fm}^{-3}$, keeping the saturation energy fixed at $E(\rho_0) = -16$ MeV. The two LO results from the chiral potentials with $\Lambda = 450$ MeV and 500 MeV are shown in black and give the lowest values of both S_0 and L in the range $26\,\mathrm{MeV} < S_0 < 29\,\mathrm{MeV}$ and $15\,\mathrm{MeV} < L < 25\,\mathrm{MeV}$. The NLO results are shown in blue and give the largest values of the isospin-asymmetry energy and its slope parameter: $34\,\mathrm{MeV} < S_0 < 36\,\mathrm{MeV}$ and $70\,\mathrm{MeV} < L < 80\,\mathrm{MeV}$. Finally, the five equations of state at N3LO* give the S_0 and L values shown in red, which are in very good agreement with the results from previous microscopic calculations [28,29].

In Fig. 10 we have also drawn S_0 vs L correlation ellipses at the 95% confidence level including only the N3LO* results

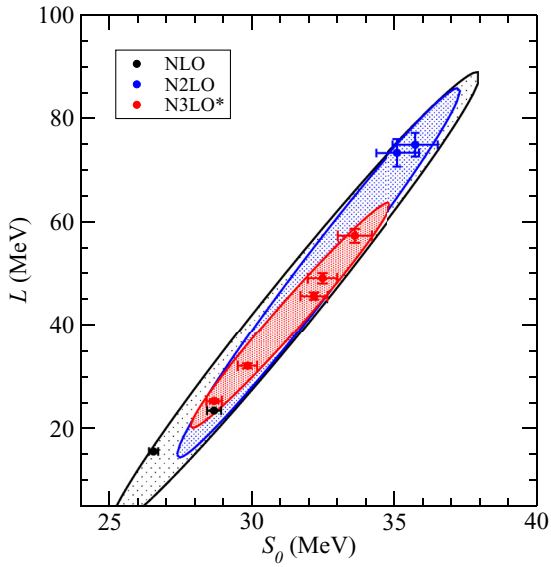

FIG. 10. 95% confidence bands for the S_0 vs L correlation at order N3LO* from chiral two- and three-nuclear forces (shown in red) and including also the NLO (gray) and N2LO (blue) points.

(shown in red) as well as including the values of S_0 and L from the NLO and N2LO equations of state. From the N3LO* correlation ellipse we infer a value of the isospin-asymmetry energy in the range $28\,\text{MeV} < S_0 < 35\,\text{MeV}$ and a slope parameter in the range $20\,\text{MeV} < L < 65\,\text{MeV}$. The upper and lower data points in the N3LO* band come from including the uncertainty due to missing physics, which effectively introduces an additional error in the theoretical prediction of the isospin-asymmetry energy on the order of $\Delta S_0 = \pm 2\,\text{MeV}$. For the slope parameter, the effect of missing physics is to extend the theory prediction by about $\Delta L = \pm 10\,\text{MeV}$. More conservative estimates on the S vs L correlation are obtained by replacing the upper and lower N3LO* points by those from the NLO and N2LO equations of state, and the resulting correlation ellipses are shown in gray and blue in Fig. 10. The parameters associated with the three correlation ellipses are given in Table II. Remarkably the inclusion of NLO and N2LO equations of state modifies only slightly the inclination angle of the correlation ellipse, indicating a robust uncertainty estimate.

In passing we note that the analytical calculation of the third-order ring diagrams from an S-wave contact interaction

TABLE II. Parameters of the S vs L correlation ellipses (at 95% confidence level) obtained at order N3LO* and including also the NLO and N2LO points. The center values are labeled S_0 and L_0, the semimajor and semiminor axes are labeled a and b, and the inclination angle is labeled θ.

	S_0 (MeV)	L_0 (MeV)	a (MeV)	b (MeV)	$\tan\theta$
N3LO*	31.3	41.9	22.2	0.64	6.37
N2LO − N3LO*	32.3	50.0	36.0	0.86	7.32
NLO − N3LO*	31.5	44.8	44.5	1.10	6.91

$V_{\rm ct} = -\frac{\pi}{M}[a_s + 3a_t + (a_t - a_s)\vec{\sigma}_1 \cdot \vec{\sigma}_2]$ provides also a check on the validity of the (commonly used) quadratic approximation in the isospin-asymmetry $\delta = (\rho_n - \rho_p)/\rho$. Introducing a pn-mixed polarization function and expanding all occurring terms up to order δ^2, one finds the following exact expression for the quadratic isospin-asymmetry energy:

$$S_2(\rho) = \frac{k_f^5}{\pi^4 M}\big(3.5124\,a_s^3 + 11.092 a_s^2 a_t + 10.137 a_s a_t^2 - 5.1014 a_t^3\big). \quad (18)$$

On the other hand the difference between the neutron matter and the nuclear matter energy per particle [see Eqs. (13) and (14)] gives

$$E_n(\rho) - E(\rho) = \frac{k_f^5}{\pi^4 M}\big(3.6330 a_s^3 + 9.4333 a_s^2 a_t + 9.4333 a_s a_t^2 - 5.2407 a_t^3\big). \quad (19)$$

One observes that the numerical coefficients of the cubic terms $a_{s,t}^3$ agree within 3%, whereas those of the interference terms are underestimated by 7% and 15% in the quadratic approximation. Moreover, when continuing the expansion in δ further one encounters a nonanalytical term of the form $\delta^4 \ln|\delta|$. It has also been found in a second-order calculation with $V_{\rm ct}$ in Ref. [57].

IV. SUMMARY AND CONCLUSIONS

We have computed the equation of state of symmetric nuclear matter and pure neutron matter including all diagrams of many-body perturbation theory up to third-order with intermediate-state energies calculated self-consistently at second-order. We have derived semi-analytical results for the third-order particle-hole ring diagrams from model-type interactions that provide valuable benchmarks for numerical calculations based on a partial-wave decomposition. We then employed realistic chiral two- and three-nucleon forces constructed at different orders in the chiral expansion together with a range of momentum-space cutoffs Λ to compute the energy per particle of symmetric matter and pure neutron matter, $E(\rho)$ and $E_n(\rho_n)$. The main motivation is to provide improved theoretical uncertainty estimates on the isospin-asymmetry energy S_0 at saturation density and its associated slope parameter L. We find that the convergence in many-body perturbation theory for the neutron matter equation of state is well under control at third-order, and variations due to the choice of resolution scale are also relatively small up to $\rho = 0.25\,\text{fm}^{-3}$. The largest theoretical uncertainty comes from higher-order contributions in the chiral expansion, which we estimate by comparison of the equations of state from NLO and N2LO chiral potentials. The derived correlation bands between S_0 and L can be used in updated global analyses of the density-dependent isospin-asymmetry energy $S(\rho)$.

[1] J. M. Lattimer and M. Prakash, Phys. Rep. **333-334**, 121 (2000).
[2] A. W. Steiner, M. Prakash, J. M. Lattimer, and P. J. Ellis, Phys. Rep. **411**, 325 (2005).
[3] J. M. Lattimer and M. Prakash, Phys. Rep. **442**, 109 (2007).
[4] P. Danielewicz, R. Lacey, and W. G. Lynch, Science **298**, 1592 (2002).
[5] J. B. Natowitz, G. Röpke, S. Typel, D. Blaschke, A. Bonasera, K. Hagel, T. Klähn, S. Kowalski, L. Qin, S. Shlomo, R. Wada, and H. H. Wolter, Phys. Rev. Lett. **104**, 202501 (2010).
[6] L. Qin *et al.*, Phys. Rev. Lett. **108**, 172701 (2012).
[7] C. J. Horowitz, E. F. Brown, Y. Kim, W. G. Lynch, R. Michaels, A. Ono, J. Piekarewicz, M. B. Tsang, and H. H. Wolter, J. Phys. G: Nucl. Part. Phys. **41**, 093001 (2014).
[8] S. Weinberg, Phys. A **96**, 327 (1979).
[9] E. Epelbaum, H.-W. Hammer, and U.-G. Meißner, Rev. Mod. Phys. **81**, 1773 (2009).
[10] R. Machleidt and D. R. Entem, Phys. Rep. **503**, 1 (2011).
[11] S. K. Bogner, T. T. S. Kuo, and A. Schwenk, Phys. Rep. **386**, 1 (2003).
[12] S. Bogner, R. Furnstahl, and A. Schwenk, Prog. Part. Nucl. Phys. **65**, 94 (2010).
[13] F. Sammarruca, L. Coraggio, J. W. Holt, N. Itaco, R. Machleidt, and L. E. Marcucci, Phys. Rev. C **91**, 054311 (2015).
[14] E. Epelbaum, H. Krebs, and U.-G. Meißner, Eur. Phys. J. A **51**, 53 (2015).
[15] S. K. Bogner, A. Schwenk, R. J. Furnstahl, and A. Nogga, Nucl. Phys. A **763**, 59 (2005).
[16] K. Hebeler and A. Schwenk, Phys. Rev. C **82**, 014314 (2010).
[17] S. Fritsch, N. Kaiser, and W. Weise, Nucl. Phys. A **750**, 259 (2005).
[18] K. Hebeler, S. K. Bogner, R. J. Furnstahl, A. Nogga, and A. Schwenk, Phys. Rev. C **83**, 031301 (2011).
[19] L. Coraggio, J. W. Holt, N. Itaco, R. Machleidt, and F. Sammarruca, Phys. Rev. C **87**, 014322 (2013).
[20] L. Coraggio, J. W. Holt, N. Itaco, R. Machleidt, L. E. Marcucci, and F. Sammarruca, Phys. Rev. C **89**, 044321 (2014).
[21] E. Epelbaum, H. Krebs, D. Lee, and U. G. Meißner, Eur. Phys. J. A **40**, 199 (2009).
[22] A. Gezerlis, I. Tews, E. Epelbaum, S. Gandolfi, K. Hebeler, A. Nogga, and A. Schwenk, Phys. Rev. Lett. **111**, 032501 (2013).
[23] M. Kohno, Phys. Rev. C **88**, 064005 (2013).
[24] A. Roggero, A. Mukherjee, and F. Pederiva, Phys. Rev. Lett. **112**, 221103 (2014).
[25] A. Carbone, A. Rios, and A. Polls, Phys. Rev. C **90**, 054322 (2014).
[26] G. Hagen, T. Papenbrock, A. Ekström, K. A. Wendt, G. Baardsen, S. Gandolfi, M. Hjorth-Jensen, and C. J. Horowitz, Phys. Rev. C **89**, 014319 (2014).
[27] G. Wlazłowski, J. W. Holt, S. Moroz, A. Bulgac, and K. J. Roche, Phys. Rev. Lett. **113**, 182503 (2014).
[28] K. Hebeler, J. M. Lattimer, C. J. Pethick, and A. Schwenk, Phys. Rev. Lett. **105**, 161102 (2010).
[29] S. Gandolfi, J. Carlson, and S. Reddy, Phys. Rev. C **85**, 032801 (2012).
[30] J. M. Lattimer and Y. Lim, Astrophys. J. **771**, 51 (2013).
[31] J. M. Lattimer and A. W. Steiner, Eur. Phys. J. A **50**, 40 (2014).
[32] I. Tews, S. Gandolfi, A. Gezerlis, and A. Schwenk, Phys. Rev. C **93**, 024305 (2016).
[33] C. Drischler, A. Carbone, K. Hebeler, and A. Schwenk, Phys. Rev. C **94**, 054307 (2016).
[34] T. Krüger, I. Tews, K. Hebeler, and A. Schwenk, Phys. Rev. C **88**, 025802 (2013).
[35] E. Rrapaj, A. Roggero, and J. W. Holt, Phys. Rev. C **93**, 065801 (2016).
[36] G. F. Bertsch and T. T. S. Kuo, Nucl. Phys. A **112**, 204 (1968).
[37] J. W. Holt, N. Kaiser, and W. Weise, Nucl. Phys. A **870-871**, 1 (2011).
[38] J. W. Holt, N. Kaiser, and W. Weise, Nucl. Phys. A **876**, 61 (2012).
[39] D. R. Entem and R. Machleidt, Phys. Rev. C **68**, 041001 (2003).
[40] L. Coraggio, A. Covello, A. Gargano, N. Itaco, D. R. Entem, T. T. S. Kuo, and R. Machleidt, Phys. Rev. C **75**, 024311 (2007).
[41] E. Marji, A. Canul, Q. MacPherson, R. Winzer, C. Zeoli, D. R. Entem, and R. Machleidt, Phys. Rev. C **88**, 054002 (2013).
[42] D. Davesne, J. W. Holt, A. Pastore, and J. Navarro, Phys. Rev. C **91**, 014323 (2015).
[43] C. Wellenhofer, J. W. Holt, and N. Kaiser, Phys. Rev. C **93**, 055802 (2016).
[44] J. W. Holt, N. Kaiser, and W. Weise, Prog. Part. Nucl. Phys. **73**, 35 (2013).
[45] J. W. Holt, M. Rho, and W. Weise, Phys. Rep. **621**, 2 (2016).
[46] J. W. Holt, N. Kaiser, and W. Weise, Phys. Rev. C **79**, 054331 (2009).
[47] G. Hagen, T. Papenbrock, D. J. Dean, A. Schwenk, A. Nogga, M. Włoch, and P. Piecuch, Phys. Rev. C **76**, 034302 (2007).
[48] I. Tews, T. Krüger, K. Hebeler, and A. Schwenk, Phys. Rev. Lett. **110**, 032504 (2013).
[49] N. Kaiser, Eur. J. Phys. A **48**, 58 (2012).
[50] J. W. Holt, N. Kaiser, G. A. Miller, and W. Weise, Phys. Rev. C **88**, 024614 (2013).
[51] J. W. Holt, N. Kaiser, and G. A. Miller, Phys. Rev. C **93**, 064603 (2016).
[52] F. D. Becchetti and G. W. Greenless, Phys. Rev. **182**, 1190 (1969).
[53] R. L. Varner, W. J. Thompson, T. L. McAbee, E. J. Ludwig, and T. B. Clegg, Phys. Rep. **201**, 57 (1991).
[54] A. J. Koning and J. P. Delaroche, Nucl. Phys. A **713**, 231 (2003).
[55] C. Wellenhofer, J. W. Holt, and N. Kaiser, Phys. Rev. C **92**, 015801 (2015).
[56] D. R. Entem, N. Kaiser, R. Machleidt, and Y. Nosyk, Phys. Rev. C **91**, 014002 (2015).
[57] N. Kaiser, Phys. Rev. C **91**, 065201 (2015).